



# Hydro-mechanical coupled mechanisms of hydraulic fracture propagation in rocks with cemented natural fractures



Zhiqiang Chen<sup>a</sup>, Zhengming Yang<sup>b</sup>, Moran Wang<sup>a,\*</sup>

<sup>a</sup> Department of Engineering Mechanics and CNMM, Tsinghua University, Beijing 100084, China

<sup>b</sup> PetroChina Research Institute of Petroleum Exploration & Development, Langfang, Hebei 065007, China

## ARTICLE INFO

### Keywords:

Hydraulic fracture  
Cemented fracture  
Natural fracture  
LBM-DEM

## ABSTRACT

Natural fractures commonly exist in unconventional reservoirs such as shale and tight gas sandstone, which are mostly cemented (or sealed) with minerals and not able to contribute to reservoir storage or rock permeability. However, during hydraulic fracture stimulation, these cemented natural fractures will be encountered and influence hydraulic fracture geometry greatly and, thereby, gas production. In this work, hydraulic fracture propagation in rock with cemented natural fracture is investigated using our recently developed and validated hydro-mechanical coupled LBM-DEM model. The numerical results show that both the strength ratio (between cemented natural fracture and host rock) and the approach angle (between hydraulic and cemented natural fracture) significantly affect the hydraulic fracture propagation. A larger strength contrast or a smaller approach angle will be more conducive to deflection, which is consistent with experimental observation. For rocks with weakly cemented natural fractures, deflection is mainly caused by shear failure in weakly cemented fracture. However, for rocks with strongly cemented natural fractures, deflection happens accompanying with tensile failure in host rock along the cement wall, which cannot be captured by the previous numerical models where the cemented natural fracture is treated as a bonded interface. In addition, complex fracture network is more easily formed if multiple weakly cemented natural fractures are orthogonal to the hydraulic fracture propagation direction.

## 1. Introduction

Hydraulic fracture is an indispensable technique to stimulate oil or gas reservoirs especially for unconventional ones (Economides and Nolte, 2000). For conventional reservoirs, single planar hydraulic fracture is enough to improve well production. However, for unconventional ones only complex fracture network can achieve economic extraction owing to their low permeability (Mayerhofer et al., 2010), which brings in the challenge for both hydraulic fracture treatments and understanding the involved mechanism (Warpinski and Teufel, 1987).

Natural fractures caused by complex sedimentary process, tectonic activities or reservoir pressure change are ubiquitous in unconventional reservoirs (i.e. shale and tight gas sandstone etc.) (Gale et al., 2007, 2014), which are mostly cemented (or sealed) with different minerals. In many reservoirs, cemented natural fractures serve as barriers, when they are encountered, hydraulic fracture will be blocked from further propagation (Warpinski and Teufel, 1987). However, in some other reservoirs, hydraulic fracture can stimulate cemented natural fractures to reactivate, forming a complex fracture network (Fisher et al., 2002; Gale et al.,

2007; Maxwell et al., 2002). Thus, cemented natural fractures in unconventional reservoirs greatly affect the hydraulic fracture treatment, which results in some production anomalies that cannot be readily explained by hydro-fracturing stimulation of host rock alone (Gale et al., 2014). However, mechanisms of hydraulic fracture propagation in rock with cemented natural fractures have not been well understood yet (Gale et al., 2014).

In the past few decades, a lot of experimental, analytical and numerical efforts have been made to explore the influence of natural fracture on hydraulic fracture (Blanton, 1982; Gu et al., 2012; Renshaw and Pollard, 1995; Warpinski and Teufel, 1987; Weng et al., 2011), trying to understand the underlying physics and provide suggestions for hydraulic fracture optimization. In these investigations, natural fracture is usually treated as a frictional interface with zero thickness. Experimental results show that geologic discontinuity (frictional interface) significantly affects the hydraulic fracture geometry (Warpinski and Teufel, 1987) and the approach angle of hydraulic fracture and natural fracture also plays an important role in this process (Blanton, 1982). Renshaw and Pollard (1995) proposed an analytical criterion to predict hydraulic fracture

\* Corresponding author.

E-mail address: [mrwang@tsinghua.edu.cn](mailto:mrwang@tsinghua.edu.cn) (M. Wang).

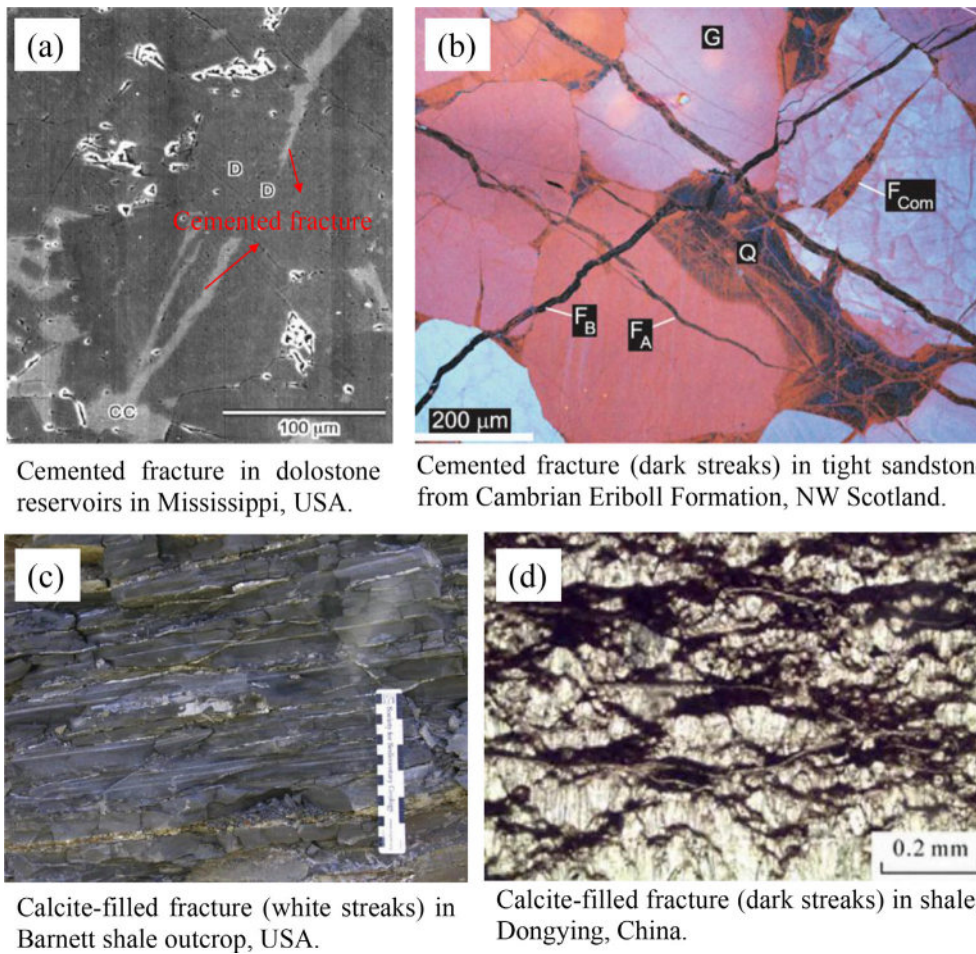


**Fig. 1.** Cemented natural fractures in unconventional reservoirs. (a) Cemented fracture in dolostone reservoir Mississippi, USA, where light gray streaks are fractures filled by dolomite and calcite (Gale et al., 2004). (b) Cemented fractures in tight sandstone from Cambrian Eriboll Formation, NW Scotland, where dark lines are fractures filled by quartz (Laubach and Diaz-Tushman, 2009). (c) Calcite-filled fracture (white streaks) in Barnett shale outcrop USA (Gasparrini et al., 2014). (d) Cemented fractures in shale from Dongying China, where the dark streaks are fractures filled with calcite (Cunfei et al., 2016).

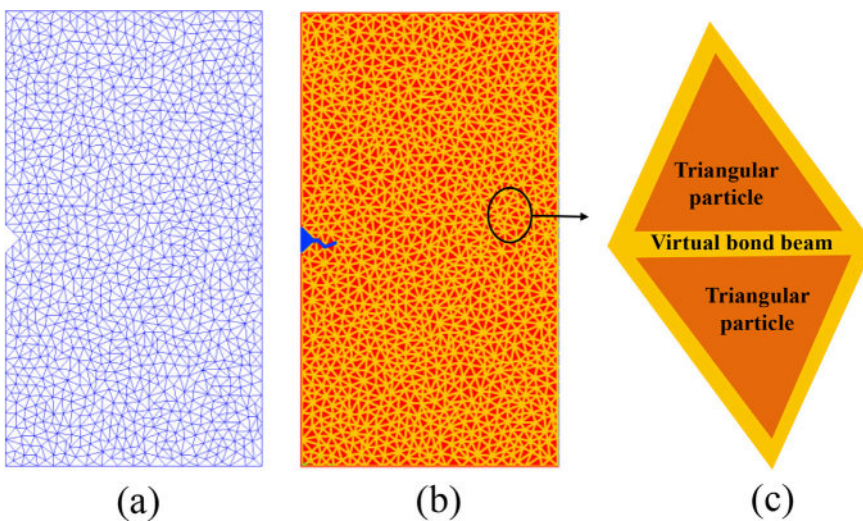


**Fig. 2.** Schematic for LBM-DEM simulation of hydraulic fracture. (a) Discretization of the rock sample by triangle particles, where a hole is set in the left edge for fluid injection. (b) Diagram of fluid channel (yellow part) in rock, where an initial crack (blue part) is introduced to guide the subsequent hydraulic fracture propagation. (c) Partial enlarged view for two bonded particles separated by the virtual bond beam that serves as flow channel for fluid. (For interpretation of the references to color in this figure legend, the reader is referred to the Web version of this article.)

interaction with unbounded frictional interface orthogonally. Gu et al. (2012) extended this criterion to the nonorthogonal case.

In the above researches, natural fracture was treated as a frictional interface, but according to the core and outcrop observation, natural fractures in unconventional reservoirs are largely cemented by different minerals with a certain thickness ranging from hundreds of micrometers to several millimeters (Gale et al., 2007) (see Fig. 1). In Barnett Shale,

most natural fractures are filled with calcite, which is weaker than the shale matrix. However, in Woodford Formation, the filling material is quartz, which is stronger than the host rock (Gale and Holder, 2010). Compared with frictional interface, cemented fracture has a more complex influence on hydraulic fracture as reported in some experiments (Bahorich et al., 2012; Olson et al., 2012), and this complexity arises from two aspects. Firstly, cemented fracture can accommodate tensile

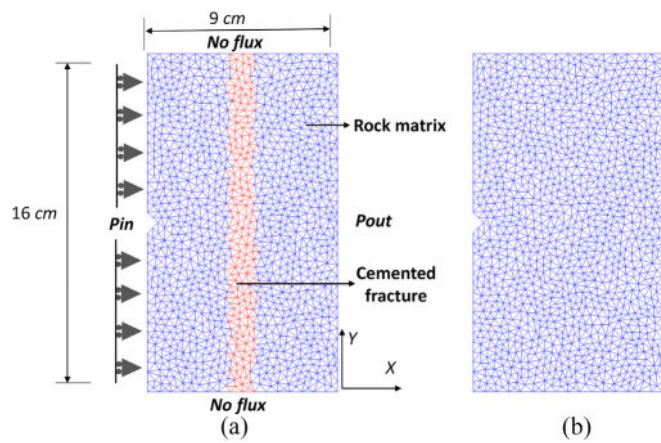


Fig. 3. The computation domain and boundary conditions for modeling hydraulic fracture propagation in (a) rock with cemented natural fracture, (b) a homogeneous rock.

Table 1  
DEM parameters in current model.

| Parameters                                    | Value                         |
|---|-------------------------------|
| Normal stiffness, $K_n$                       | $1 \times 10^6 \text{ N/m}$   |
| Tangential stiffness, $K_t$                   | $6.7 \times 10^5 \text{ N/m}$ |
| Particle friction coefficient, $\mu_{fric}$   | 0.4                           |
| Normal elastic modulus, $M_n^{cohe}$          | $5.0 \times 10^7 \text{ Pa}$  |
| Tangential elastic modulus, $M_t^{cohe}$      | $5.0 \times 10^7 \text{ Pa}$  |
| Rock matrix bonding strength, $\epsilon_{th}$ | 0.012                         |

Table 2  
LBM parameters in current model.

| Parameters                       | Value                                     |
|----------------------------------|---|
| Fluid density, $\rho$            | $1 \times 10^3 \text{ kg/m}^3$            |
| Fluid kinematic viscosity, $\nu$ | $2.0 \times 10^{-3} \text{ m}^2/\text{s}$ |
| Lattice size in LBM, $\delta_x$  | $1.0 \times 10^{-4} \text{ m}$            |
| Time step in LBM, $\delta_t$     | $2.0 \times 10^{-7} \text{ s}$            |

stress at both tangential and normal directions to itself owing to the cohesion of cement material. Secondly, at least two parallel interfaces exist in rock with cemented fracture (Virgo et al., 2013). This means the conclusion obtained from hydraulic fracture propagation in rock with frictional interface cannot be directly applied to the cemented fracture cases. In addition, analytical prediction of hydraulic fracture interaction with cemented fracture is very difficult especially for nonorthogonal cases (Virgo et al., 2013).

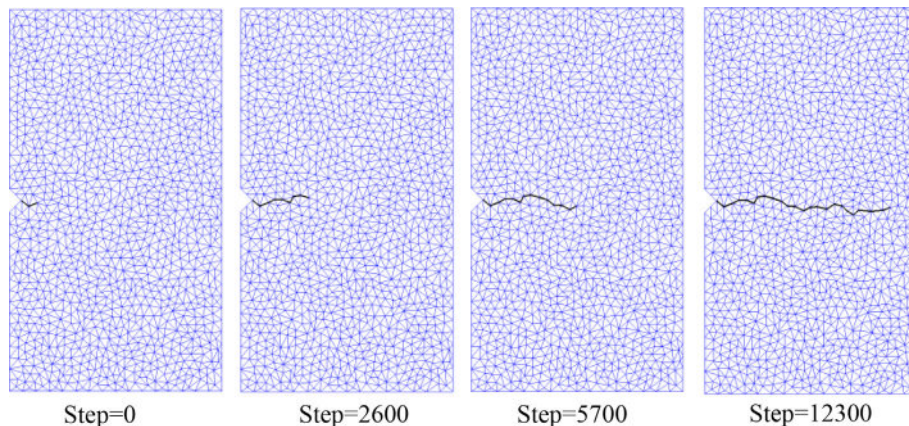


Fig. 4. Hydraulic fracture propagation in a homogeneous rock, where no cemented natural fracture exists.

Therefore, some researchers attempted to examine the nature of hydraulic fracture propagation in rock with cemented natural fractures experimentally (Bahorich et al., 2012; Wang et al., 2017). Olson et al. (2012, 2016) embedded different discontinuities into a rock sample as proxies for cemented natural fractures, and found both property contrast and approach angle affected the interaction process (Alabbad and Olson, 2016; Bahorich et al., 2012). Wang et al. (2017) considered the strength contrast effect in this process, and found that deflection more easily happened in rocks with weakly cemented natural fractures (Wang et al., 2017).

Recently, discrete element method (DEM) has achieved great success in simulating complex fracturing behavior in granular material (Behratar et al., 2017; Galindo-Torres et al., 2012), which provides a promising approach to explore the underlying physics of hydraulic fracture propagation in rocks with cemented natural fractures. Mechanically induced fracture propagation in rocks with cemented natural fractures (or veins) has been simulated using DEM, where the extension fracture is driven by the external tensile, compressive or bending force, respectively (Lee et al., 2016; Virgo et al., 2013, 2014). However, the comprehensive numerical investigation of hydraulic fracture propagation in rock with cemented natural fracture is relatively little. In our previous work, we developed a hydro-mechanical coupled LBM-DEM model to simulate hydraulic fracture process, where solid deformation and fracturing behavior were modeled by DEM and fluid flow was solved by lattice Boltzmann method (LBM) directly (Chen and Wang, 2017). Compared with the traditional continuum-based models, LBM-DEM model can simulate complex fracturing process explicitly, and hydraulic force can be calculated accurately without empirical parameters.

Thus, the aim of present work is to study the hydraulic fracture propagation in rock with cemented natural fracture with particular emphasis on the influence of strength ratio (between cemented fracture and host rock) and approach angle (between hydraulic and cemented natural fracture). It is motivated by the fact that natural fractures in unconventional reservoirs are often cemented by different minerals, which may be weaker or stronger than the host rock. These cemented natural fractures are encountered during hydraulic fracture stimulation, and interact with hydraulic fracture at different approach angles, which influences the induced fracture geometry and hence the well production. We attempt to improve the mechanism understanding of hydraulic fracture propagation in rock with cemented natural fracture and provide suggestions in forming the complex fracture network in unconventional reservoirs.

The rest of this paper is organized as follows. Firstly, the numerical methods are introduced briefly in Section 2, which includes lattice Boltzmann method (LBM), discrete element method (DEM) and how they are coupled with each other. Section 3 is the numerical results and discussions, and in the last part, the paper is concluded.

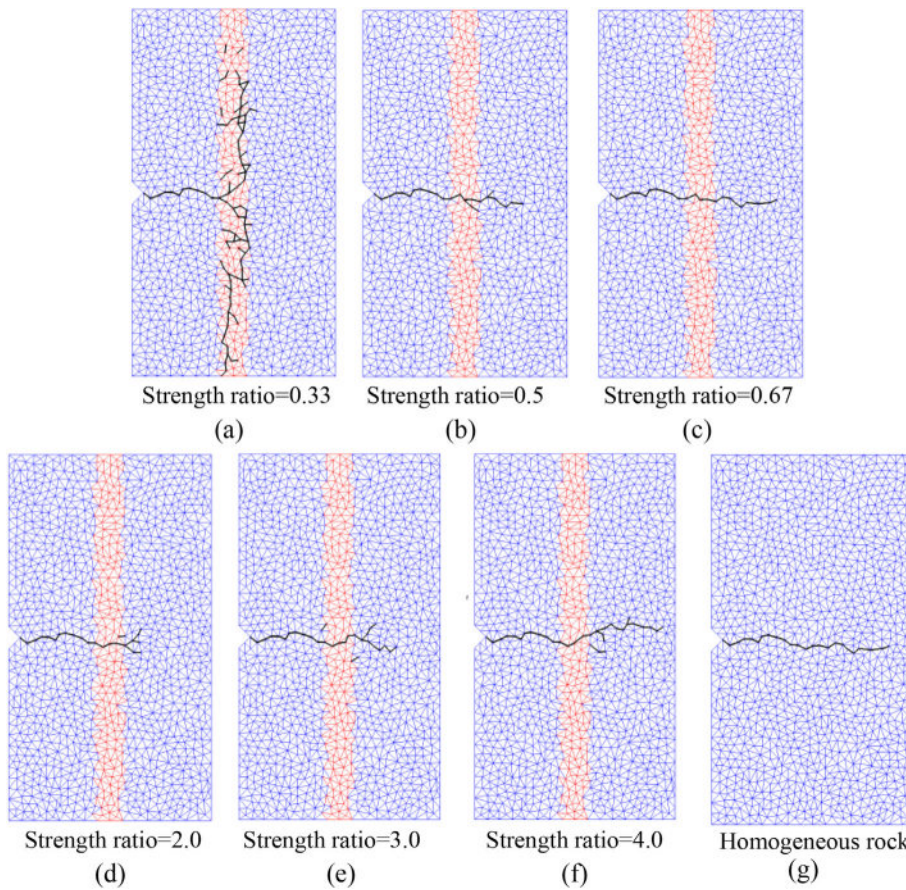


Fig. 5. Hydraulic fracture in rock with cemented natural fracture, where (a) strength ratio = 0.33, (b) strength ratio = 0.5 and (c) strength ratio = 0.67 are weakly cemented fractures; (d) strength ratio = 2.0, (e) strength ratio = 3.0 and (f) strength ratio = 4.0 are strongly cemented fractures; (g) is a homogeneous rock where no cemented natural fracture exists.

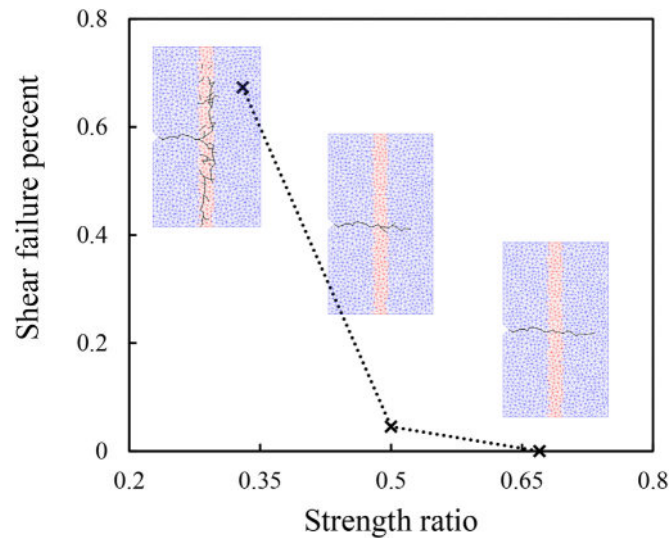


Fig. 6. Shear failure percent during hydraulic fracture propagation in rocks with weakly cemented natural fractures, which shows that shear failure dominates the deflection process.

## 2. Numerical method

A brief introduction of current LBM-DEM coupled model is presented here, and more detail technical content can be found in our recent work (Chen and Wang, 2017).

### 2.1. Discrete element method (DEM)

In current DEM model, spheropolyhedra particles are used to overcome the limitation of round particles (Galindo-Torres et al., 2012), which has achieved great success in simulating mechanical behavior of rock (Behraftar et al., 2017; Galindo-Torres et al., 2012).

To capture the bonding effect between grains in rock, cohesive forces at the common face shared by two adjacent particles are assumed, which are given by

$$\begin{cases} \mathbf{F}_n^{cohe} = M_n^{cohe} A \varepsilon_n \mathbf{n} \\ \mathbf{F}_t^{cohe} = M_t^{cohe} A \varepsilon_t \mathbf{t} \end{cases} \quad (1)$$

where  $\mathbf{F}_n^{cohe}$  and  $\mathbf{F}_t^{cohe}$  are cohesive forces,  $M_n^{cohe}$  and  $M_t^{cohe}$  are the elastic modulus of assumed bond material,  $\varepsilon_n$  and  $\varepsilon_t$  are the strains of two adjacent faces depart from each other,  $A$  is the shared face area,  $\mathbf{n}$  and  $\mathbf{t}$  are unit vectors in normal and tangential directions. Once the relative displacement of two adjacent particles reaches the threshold value  $\varepsilon_{th}$

$$\frac{|\varepsilon_n| + |\varepsilon_t|}{\varepsilon_{th}} > 1, \quad (2)$$

the cohesive forces vanish and a crack forms along the common face. The cracks are classified as shear failure ( $\varepsilon_n < \varepsilon_t$ ) or tensile failure ( $\varepsilon_n > \varepsilon_t$ ) according to the relative magnitude of tensile strain and shear strain when bond is broken.

Besides cohesive force, collision force is another particles interaction force, which is written as (Cundall and Strack 1979)

$$\begin{cases} \mathbf{F}_n^{cont} = K_n \Delta l_n \mathbf{n} \\ \mathbf{F}_t^{cont} = K_t \Delta l_t \mathbf{t} \end{cases} \quad (3)$$

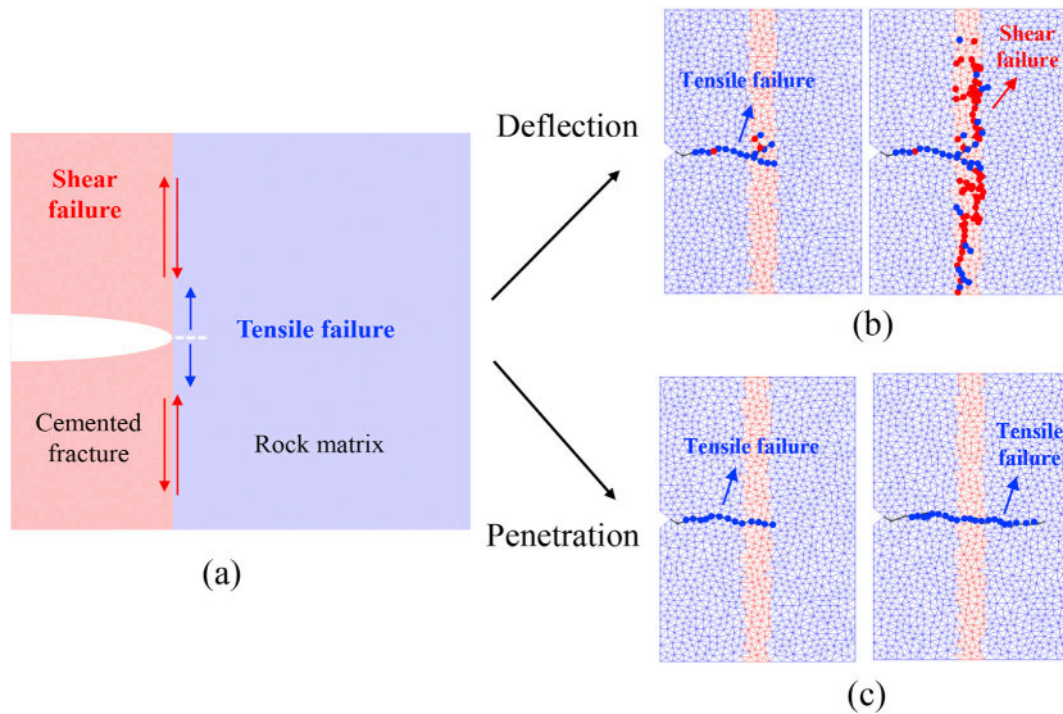


Fig. 7. Deflection and penetration process in rocks with weakly cemented fractures. (a) Schematic to show the underlying physics controlling the hydraulic fracture interaction with weakly cemented fracture. (b) Hydraulic fracture evolution and failure mechanism in rock with strength ratio being 0.33 and (c) 0.67, where red and blue dots are cracks caused by shear and tensile force, respectively.

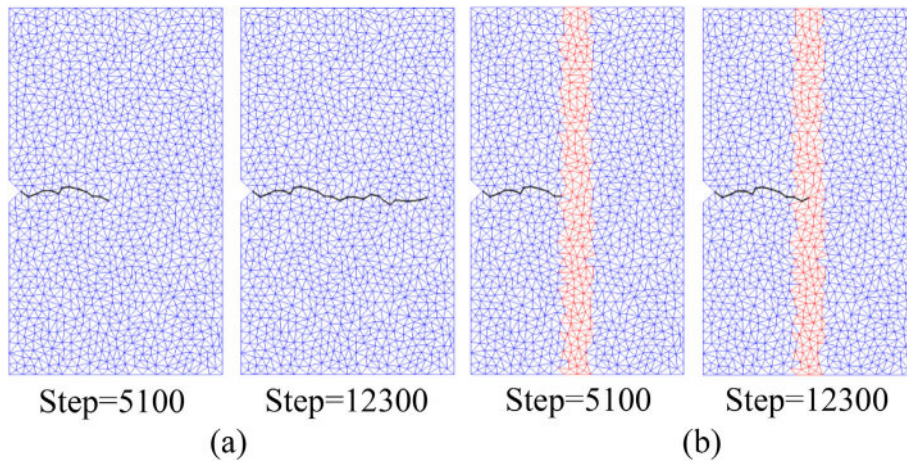


Fig. 8. Hydraulic fracture evolution in (a) a homogeneous rock, and (b) rock with strongly cemented natural fracture (strength ratio = 4.0).

where  $F_n^{cont}$  and  $F_t^{cont}$  are collision forces,  $K_n$  and  $K_t$  are spring stiffness,  $\Delta l_n$  and  $\Delta l_t$  are the overlapping lengths in normal and tangential directions respectively.

### 2.2. Lattice Boltzmann method (LBM)

Lattice Boltzmann method (LBM) is an efficient method to simulate mass, momentum and energy transfer process (i.e. fluid flow, diffusion, and heat transfer, etc.) with complicated boundary conditions (He et al., 2017; Wang et al., 2007, 2016) or multiphase interfaces (Xie et al., 2016). Recently, LBM has been coupled with DEM to investigate the hydro-mechanical coupled process in geophysical system owing to its good performance in capturing complex solid-fluid interaction efficiently and accurately (Boutt et al., 2011; Chen and Wang, 2017; Chen et al., 2016).

In LBM, Boltzmann equation is solved in discrete lattices, where the

basic variable is density distribution. The macroscopic parameters (velocity, pressure, etc.) obtained from density distribution obey the desired macroscopic governing equations (i.e. NS equations for fluid flow) by Chapman-Enskog expansion (Chen and Doolen, 1998). In current simulation, three dimensional 15-speed model (D3Q15) is applied. Its evolution equation is written as

$$f_i(\mathbf{x} + \mathbf{e}_i \delta_t, t + \delta_t) = f_i(\mathbf{x}, t) - \frac{1}{\tau} (f_i(\mathbf{x}, t) - f_i^{eq}(\mathbf{x}, t)), \quad i = 0 - 14, \quad (4)$$

where  $\mathbf{x}$  is the position vector,  $f_i$  is the density distribution in the  $i_{th}$  lattice discrete velocity direction  $\mathbf{e}_i$ ,  $f_i^{eq}$  is the corresponding equilibrium distribution,  $\delta_t$  is the time step. Parameter  $\tau$  is the dimensionless relaxation time related to the fluid kinematic viscosity

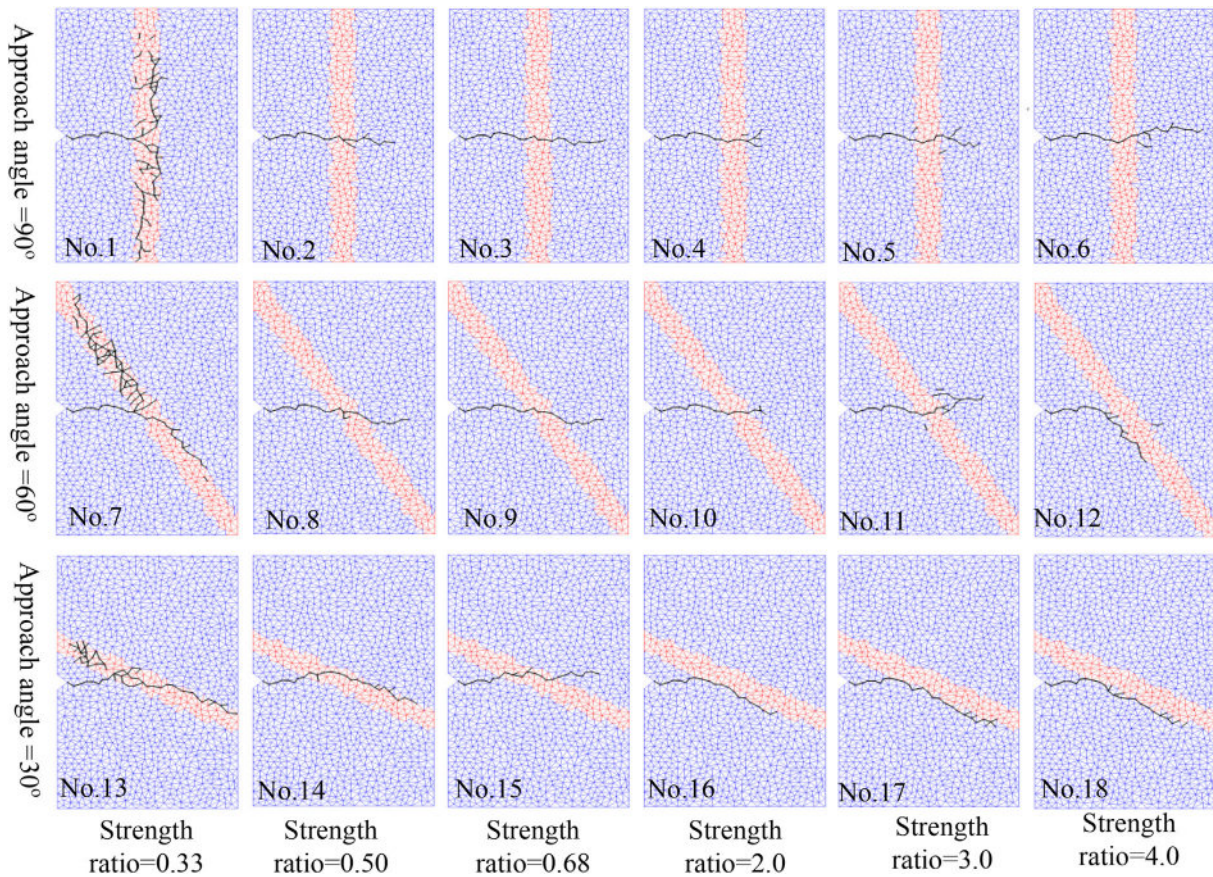


Fig. 9. Current simulation results for hydraulic fracture propagation in rocks with different strength ratios (between cemented natural fracture and host rock) at various approach angles (between hydraulic and cemented natural fracture).

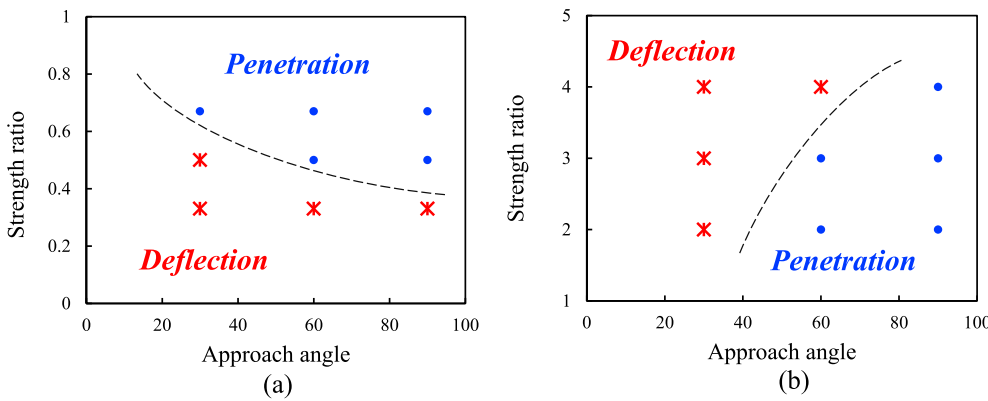


Fig. 10. Summary of strength ratio and approach angle effect on hydraulic fracture propagation in rocks with (a) weakly cemented natural fracture or (b) strongly cemented natural fracture. Red and blue dots represent deflection and penetration respectively. (For interpretation of the references to color in this figure legend, the reader is referred to the Web version of this article.)

$$\nu = \frac{(\tau - 1/2)\delta_x^2}{3\delta_t}, \tag{5}$$

where  $\delta_x$  is the lattice size. Discrete velocity  $\mathbf{e}$  has 15 directions, which are presented as

$$\mathbf{e} = c \begin{bmatrix} 0 & 1 & 0 & -1 & 0 & 0 & 0 & 1 & 1 & 1 & 1 & -1 & -1 & -1 & -1 \\ 0 & 0 & 0 & 0 & 0 & -1 & 1 & -1 & -1 & 1 & 1 & -1 & -1 & 1 & 1 \\ 0 & 0 & 1 & 0 & -1 & 0 & 0 & 1 & -1 & -1 & 1 & 1 & -1 & -1 & 1 \end{bmatrix}, \tag{6}$$

where  $c = \delta_x/\delta_t$ . The equilibrium distribution is given by

$$f_i^{eq}(\rho, \mathbf{u}) = \rho \omega_i \left[ 1 + \frac{3\mathbf{e}_i \cdot \mathbf{u}}{c^2} + \frac{9(\mathbf{e}_i \cdot \mathbf{u})^2}{2c^4} - \frac{3\mathbf{u} \cdot \mathbf{u}}{2c^2} \right], \tag{7}$$

where the weighting factors are

$$\omega_i = \begin{cases} 2/9, & i = 0 \\ 1/9, & i = 1 - 6 \\ 1/72, & i = 7 - 14 \end{cases}. \tag{8}$$

The macroscopic parameters (density and velocity) are calculated by

$$\rho = \sum_i f_i, \tag{9}$$

$$\rho \mathbf{u} = \sum_i f_i \mathbf{e}_i, \tag{10}$$

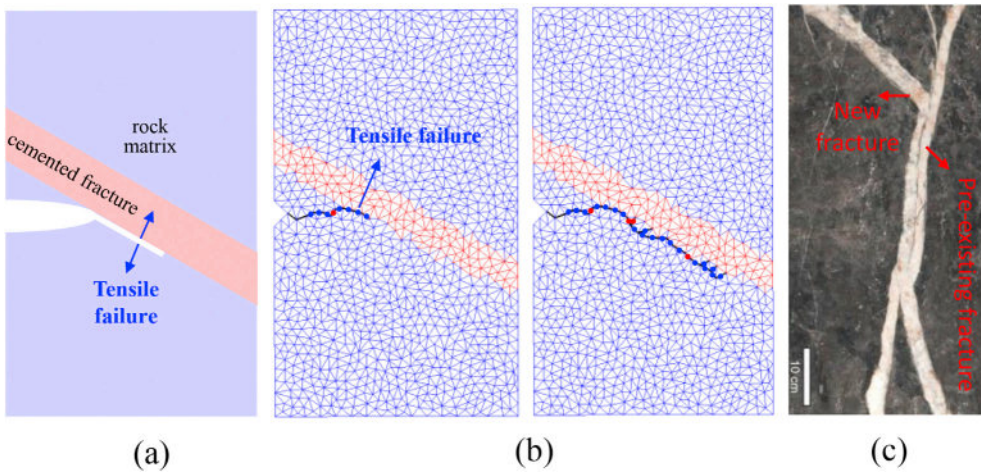


**Fig. 11.** Hydraulic fracture deflects in rocks with strongly cemented natural fracture. (a) Schematic to show the mechanism involved in this deflection process. (b) Detail hydraulic fracture evolution and failure mechanism in rock with strongly cemented natural fracture (strength ratio = 4.0), where red and blue dots are cracks caused by shear force and tensile force, respectively. (c) Deflection observed in natural structure from Oman Mountain (Virgo et al., 2013). (For interpretation of the references to color in this figure legend, the reader is referred to the Web version of this article.)

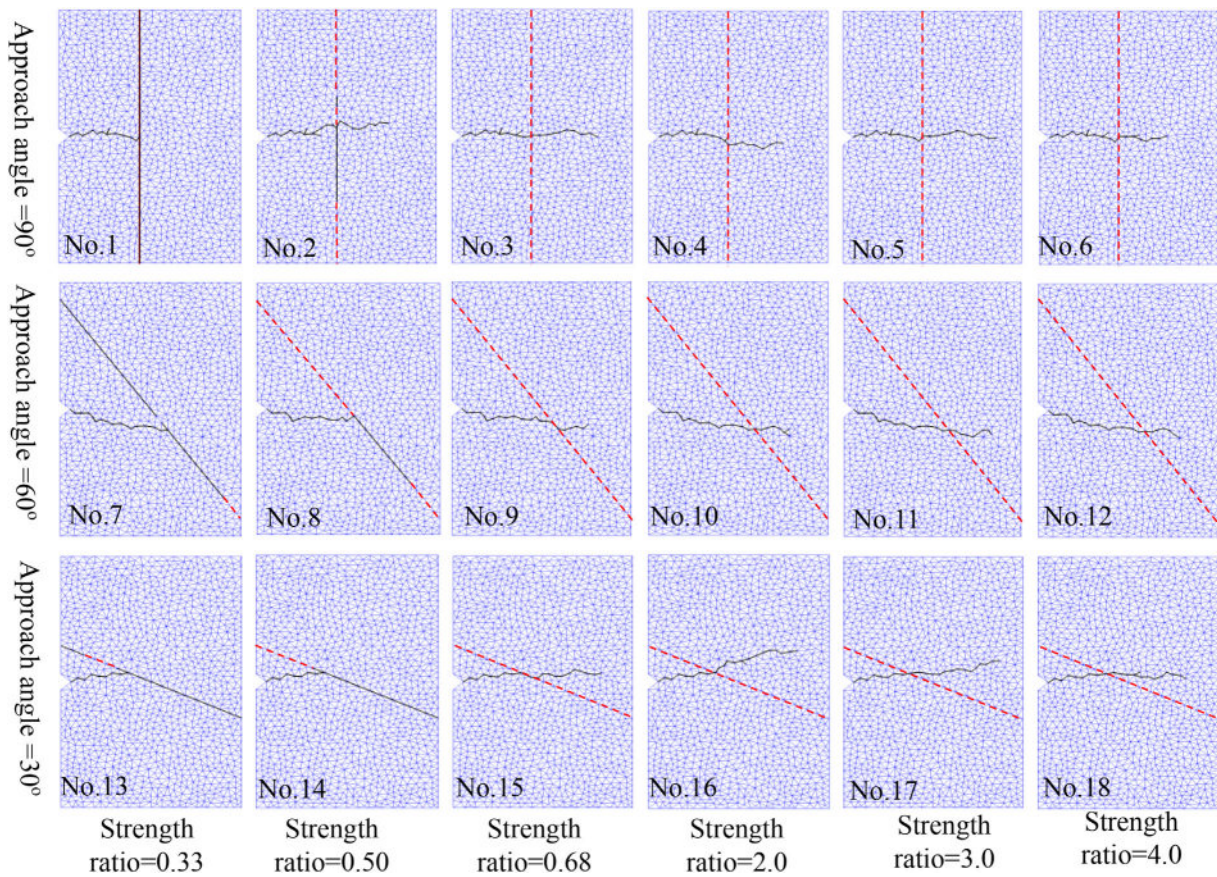


**Fig. 12.** Hydraulic fracture propagation in rocks with bonded interface, where the red dash line is bonded interface, and blue particles on both sides of bonded interface represent host rock with same mechanical properties. (For interpretation of the references to color in this figure legend, the reader is referred to the Web version of this article.)

and pressure  $p$  is given by

$$p = \frac{1}{3} \rho c^2. \tag{11}$$

**2.3. LBM-DEM coupling scheme**

In the current LBM-DEM model, immersed moving boundary (IMB) is applied to deal with fluid solid interaction at sub-grid resolution (Galindo-Torres, 2013; Noble and Torczynski, 1998; Strack and Cook,

2007). This method ensures the non-slip boundary condition for fluid flow on solid surface and allows for accurate and stable calculation of hydrodynamic force. In IMB scheme, the evolution equation in classic LBM is modified as

$$f_i(\mathbf{x} + \mathbf{e}_i \delta_t, t + \delta_t) = f_i(\mathbf{x}, t) - (1 - B) \frac{1}{\tau} (f_i(\mathbf{x}, t) - f_i^{eq}(\mathbf{x}, t)) + B \Omega_i^s. \tag{12}$$

Parameter  $\Omega$  reflects the fluid-solid interaction term, which is obtained by the bounce-back for non-equilibrium part of density distribution

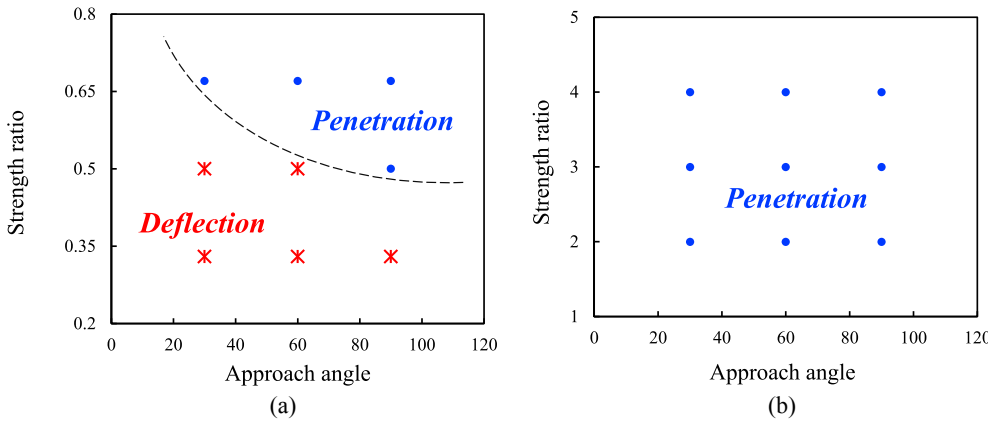


Fig. 13. Summary of hydraulic fracture propagation in rocks with (a) weakly bonded interface and (b) strongly bonded interface, where the red and blue points represent deflection and penetration process respectively. (For interpretation of the references to color in this figure legend, the reader is referred to the Web version of this article.)

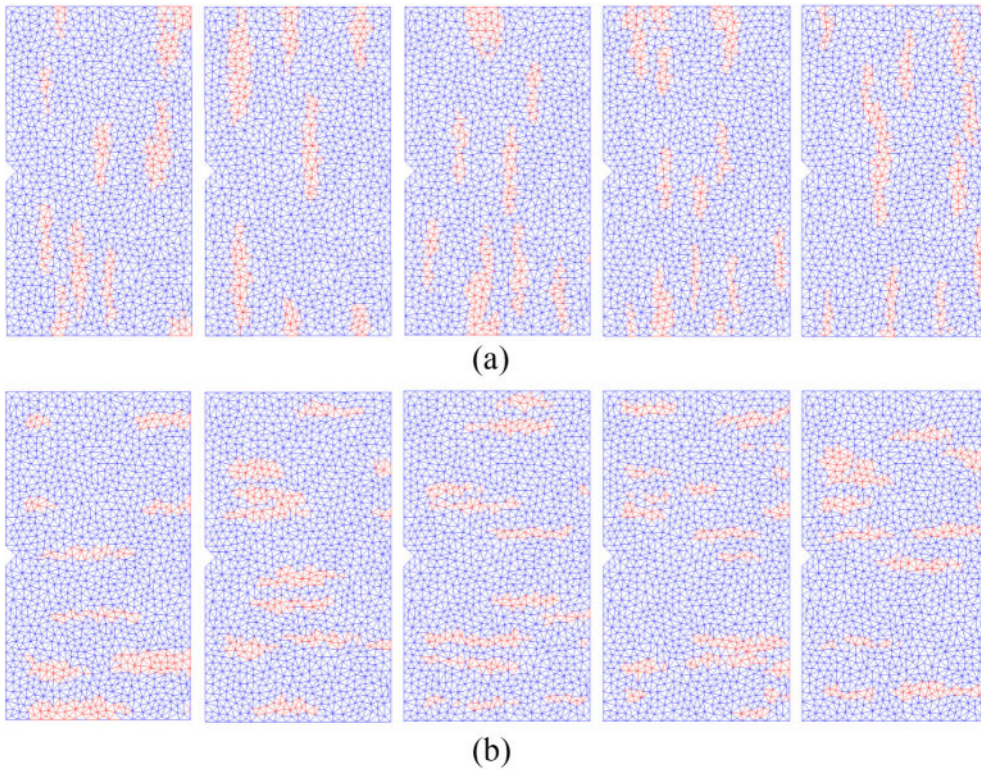


Fig. 14. Samples with multiple cemented natural fractures generated by QSGS, where cemented natural fractures are (a) orthogonal or (b) parallel to hydraulic fracture propagation direction.

$$\Omega_i^s = [f_{-i}(\mathbf{x}, t) - f_{-i}^{eq}(\rho, \mathbf{v}_p)] - [f_i(\mathbf{x}, t) - f_i^{eq}(\rho, \mathbf{v}_p)], \quad (13)$$

where  $\mathbf{v}_p$  is the solid velocity at position  $\mathbf{x}$ . Parameter  $B$  is a weighting function calculated by solid volume fraction ( $\gamma$ ) of LBM cell at position  $\mathbf{x}$

$$B = \frac{\gamma(\tau - 0.5)}{(1 - \gamma) + (\tau - 0.5)}. \quad (14)$$

Hydrodynamic force  $\mathbf{F}$  applied on solid is calculated by the momentum change of fluid covered by DEM particles

$$\mathbf{F} = \frac{\delta_x^3}{\delta_t} \sum_n B_n \left( \sum_i \Omega_i^s \mathbf{e}_i \right). \quad (15)$$

Similarly, the torque  $T$  is given by

$$\mathbf{T} = \frac{\delta_x^3}{\delta_t} \sum_n \left[ (\mathbf{x}_n - \mathbf{x}_{cm}) B_n \left( \sum_i \Omega_i^s \mathbf{e}_i \right) \right], \quad (16)$$

where  $\mathbf{x}_n$  is the fluid cell position, and  $\mathbf{x}_{cm}$  is the mass center of DEM particle.

#### 2.4. LBM-DEM simulation for hydraulic fracture

The rock in current simulations is discretized as a collection of triangular particles (see Fig. 2a), where a hole is set in the left edge for fluid injection. An initial crack is introduced near the injection hole to guide the subsequent fracture propagation (see Fig. 2b). To model fluid flow in rock, triangular particles in Fig. 2a are eroded by a small distance to obtain the flow channel (yellow part in Fig. 2b), which is a common consideration for simulating hydro-mechanical coupled process using LBM-DEM (Boutt et al., 2011). Fig. 2c is the partial enlarged view in Fig. 2b, where the inner triangular particles are impermeable and fluid can only flow along the triangular particle boundaries (termed as flow channel), which provide the basic permeability for rock matrix. This simplification can be thought of two triangular particles in Fig. 2c being

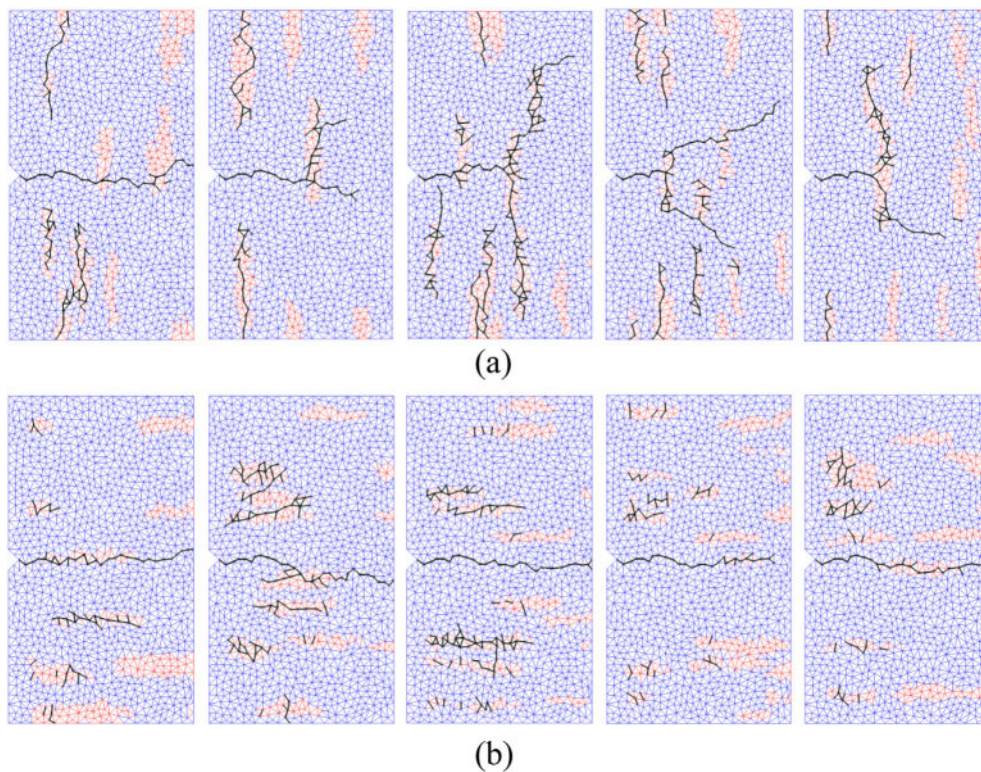


**Fig. 15.** Hydraulic fracture in rocks with multi weakly cemented natural fractures, where cemented fractures are (a) orthogonal or (b) parallel to the hydraulic fracture propagation direction.

separated by the virtual bond beam, which is permeable to fluid and able to support particle interaction force.

Fracture dependent flow conductivity is an important feature in deforming fractured rock, which means the newly formed cracks are much more permeable than the rock matrix (Zhang et al., 2002). To capture this behavior, an initial solid volume fraction ( $\gamma$ ) is introduced in the flow channel, which corresponds to a low flow conductivity. When the bond is broken, solid volume fraction in the corresponding flow channel is set to zero, which results in a high flow conductivity. By doing this, the fluid pressure fluctuation in the borehole owing to the fracture propagation can be efficiently captured. More detail about current LBM-DEM model for hydraulic fracture simulation can be found in our previous work (Chen and Wang, 2017).

### 3. Results and discussions

#### 3.1. Single cemented fracture

Natural fractures in unconventional reservoirs are largely cemented by different minerals as presented in Section 1, which results in strength contrast between cemented fracture and host rock. For shale and mudstone, calcite and quartz are two common minerals filling the natural fracture (Olson et al., 2012). Calcite has a lower strength than the shale matrix, but quartz corresponds to a higher strength. Thus, a critical question should be addressed is how the strength contrast (between cemented natural fracture and host rock) influences the hydraulic fracture propagation. In the first part of this subsection, we attempt to answer this question by comparing hydraulic fracture propagation in rocks with different strength ratios between cemented fracture and host rock. Then the effect of approach angle (between hydraulic and cemented natural fracture) is investigated, because hydraulic fracture may encounter cemented natural fractures obliquely or orthogonally in real applications. In previous numerical models, natural fracture is usually represented by a frictional or bonded interface. Thus, as a comparison, the cemented natural fracture is also treated as a bonded interface in the final part, and its effect on hydraulic fracture propagation is simulated to show the

necessity of current numerical model where cement material is represented explicitly with a certain thickness.

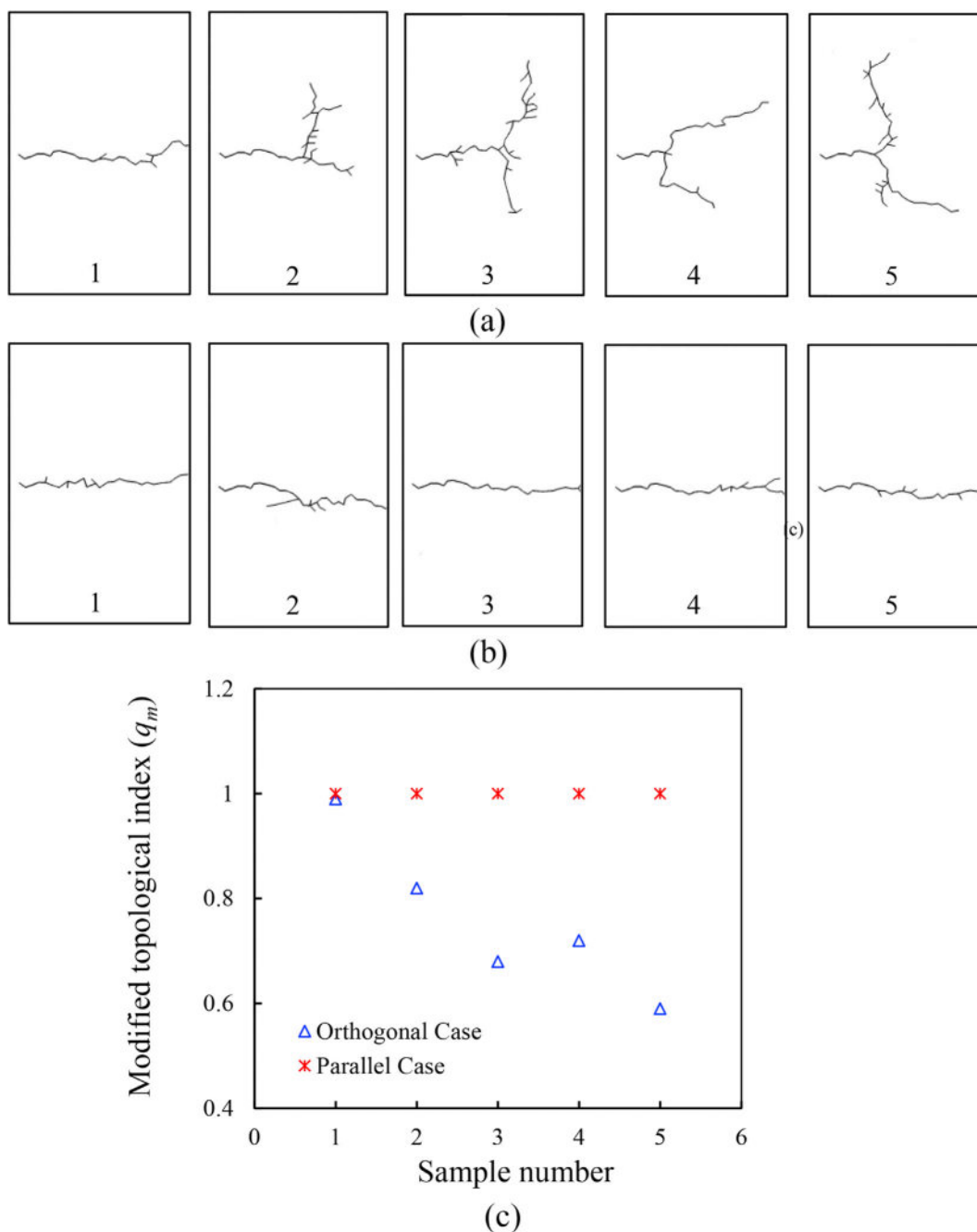
##### 3.1.1. Physical model and boundary conditions

The computation domain and boundary conditions are presented in Fig. 3a. The left edge of rock sample is set as a symmetric boundary, where DEM particles are fixed in  $x$  direction and can only move in  $y$  direction. On other three edges, rock sample is unconfined. Cemented natural fracture is generated in the sample by discretizing the cement material as a collection of bonded particles (red color in Fig. 3a) with a different tag from that in host rock, which is a common strategy to consider cemented natural fracture in DEM (Lee et al., 2016; Virgo et al., 2013, 2014). In current model, the thickness of cemented natural fracture is 10 mm and the ratio between fracture thickness and sample size is 1/9, which are reasonable and typical values used to explore the mechanism of cemented natural fracture effect on extension fracture propagation (Lee et al., 2016; Virgo et al., 2013). This work mainly focuses on the influence of strength contrast and approach angle on hydraulic fracture, and cement material thickness effect will be considered in the future. Micro parameters of particles in cement material and host rock are same except the strength value, which are listed in Table 1. In current simulation, six strength ratios (0.33, 0.5, 0.67, 2.0, 3.0, 4.0) between cement material and host rock are considered, which are classified into two groups, weakly cemented fracture (strength ratio = 0.33, 0.5, 0.67) and strongly cemented fracture (strength ratio = 2.0, 3.0, 4.0). As a comparison, hydraulic fracture propagation in a homogeneous rock without cemented natural fracture is also simulated.

To induce hydraulic fracture, a constant high fluid pressure is set on the left side of the injection hole, and a low pressure is kept on the right edge of the sample (see Fig. 3a), which is a common fluid boundary condition for hydraulic fracture simulation (Al-Busaidi et al., 2005). On upper and lower boundaries fluid velocity is zero. The fluid parameters and their LBM implementations are listed in Table 2.

##### 3.1.2. Strength contrast effect

Hydraulic fracture evolution in a homogeneous rock is presented in



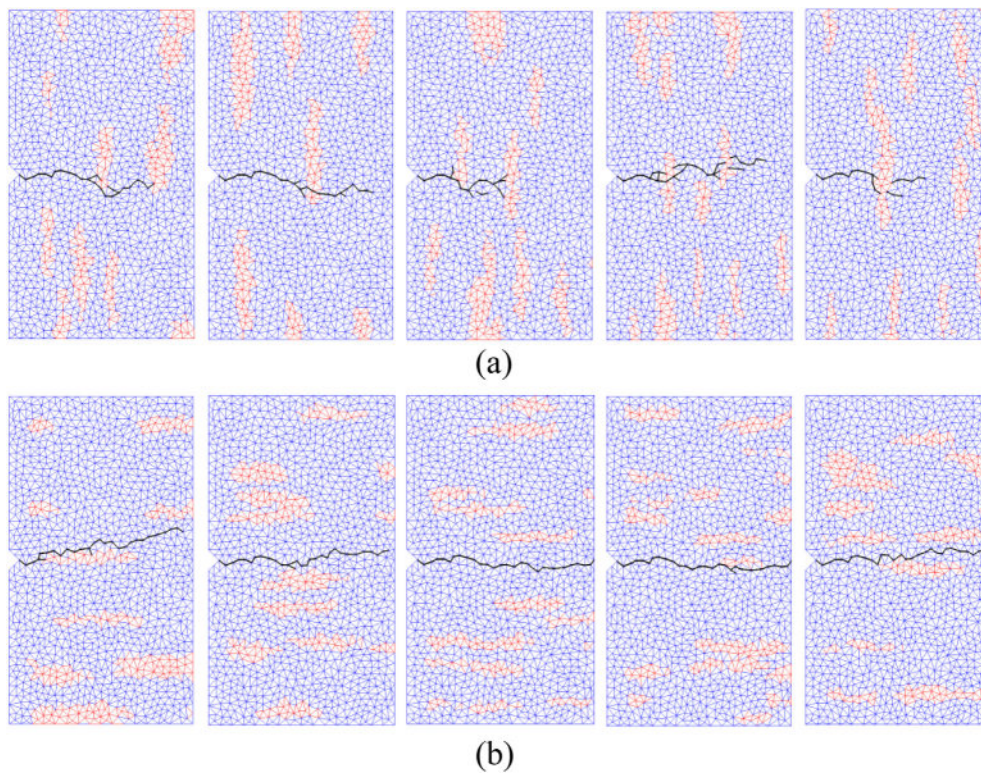
**Fig. 16.** Connected fracture networks extracted from Fig. 15 for (a) orthogonal and (b) parallel cases. (c) Modified topological indexes are calculated for fracture geometries in (a) and (b).

Fig. 4, where no cemented natural fracture exists. As expected, hydraulic fracture propagates along the x direction owing to the guidance of initial crack near the injection hole, which shows the validity of current LBM-DEM model for hydraulic fracture simulation. In addition, this result can serve as a reference to illustrate the significant effect of cemented natural fracture on hydraulic fracture propagation.

Hydraulic fracture propagation in rocks with different strength ratios between cemented natural fracture and host rock is presented in Fig. 5, where the cemented natural fracture is orthogonal to the hydraulic fracture propagation direction. In the following, influences of weakly (strength ratio = 0.33, 0.50 and 0.67) and strongly (strength ratio = 2.0, 3.0 and 4.0) cemented natural fracture on hydraulic fracture are discussed respectively.

#### A. Weakly cemented fracture

Fig. 5a–c shows the hydraulic fracture in rocks with weakly cemented natural fracture (strength ratio < 1), where two interaction processes, deflection (Fig. 5a) and penetration (Fig. 5b and c), are observed. Deflection process happens when strength ratio is equal to 0.33. In this case, hydraulic fracture bifurcates when it encounters weakly cemented natural fracture. These branches cannot penetrate into the surrounding host rock on the other side of cemented fracture, but tend to divert and propagate in weakly cemented fracture along the cemented fracture/host rock interface. As a result, hydraulic fracture is arrested by the weakly cemented fracture. With the increment of strength ratio (strength ratio = 0.5 and 0.67), interaction process shifts from deflection (Fig. 5a) to penetration (Fig. 5b and c). When strength ratio is equal to 0.67,



**Fig. 17.** Hydraulic fracture propagation in rock with multi strongly cemented natural fractures, where cemented natural fractures are (a) orthogonal or (b) parallel to the hydraulic fracture propagation direction.

weakly cemented natural fracture nearly has no influence on hydraulic fracture propagation, and the induced fracture geometry (see Fig. 5c) is just like that in a homogeneous rock (see Fig. 5g). Recently, Wang et al. (2017) also found similar results in the experiment, that weakly bonded pre-existing fracture more easily arrests the hydraulic fracture, but when the strength contrast decreases, this effect vanishes (Wang et al., 2017).

For a deeper understanding of this strength contrast controlled hydraulic fracture propagation, micro failure mechanism involved in this process is analyzed. Fig. 6 shows the percent of cracks caused by shear force in different samples (strength ratio = 0.3, 0.5 and 0.67), where deflection process accompanies with high shear failure percent. However, in penetration process, tensile failure more easily happens.

To reveal the underlying physics, hydraulic fracture evolution in deflection and penetration process are presented in Fig. 7b and c respectively. When hydraulic fracture reaches the cemented fracture/host rock interface, two possible failure mechanisms exist: tensile failure in host rock or shear failure in weakly cemented fracture (see Fig. 7a). The competition of these two failure mechanisms governs the hydraulic fracture propagation in rock with weakly cemented natural fracture. If shear failure in weakly cemented fracture occurs before tensile stress in surrounding host rock reaches its tensile strength, deflection process happens. Otherwise, penetration process happens. In rock with strength ratio being 0.33, shear slippage in weakly cemented fracture more easily happens owing to its low bonding strength, which results in the deflection process (see Fig. 7b). However, with the increment of cement strength (strength ratio = 0.67), tensile failure in host rock occurs first, so hydraulic fracture can cross the weakly cemented fracture successfully (Fig. 7c).

## B. Strongly cemented fracture

Hydraulic fractures in rocks with strongly cemented natural fractures (strength ratio = 2.0, 3.0 and 4.0) are presented in Fig. 5d–f, which show that all the hydraulic fractures can cross the strongly cemented fracture orthogonally, but compared with the result in a homogeneous rock (Fig.

5g) two differences still exist. Firstly, bifurcation happens when hydraulic fracture propagates from strongly cemented fracture to surrounding rock matrix. This feature was also observed in a recent work by Virgo et al. (2013), and they attributed this dynamic bifurcation to the acceleration of fracture tip when it propagated from a stronger into a weaker material. Secondly, when hydraulic fracture encounters strongly cemented natural fracture, accumulation of fluid pressure at the fracture tip is required to cross the strongly cemented fracture with high resistance. Thus, hydraulic fracture takes more time to propagate in rock with strongly cemented fracture than that in a homogeneous rock (see Fig. 8).

### 3.1.3. Approach angle effect

In unconventional reservoirs, cemented natural fractures trend to any directions, which may be encountered orthogonally or obliquely during hydraulic fracture treatment. Thus, it is necessary to investigate the approach angle (between hydraulic and cemented natural fracture) effect on hydraulic fracture propagation. In this part, 18 simulation cases are considered, which include 3 approach angles (30°, 60° and 90°) and 6 strength ratios (0.33, 0.5, 0.67, 2.0, 3.0 and 4.0), and the numerical results are summarized in Fig. 9.

In order to consider the influence of strength ratio and approach angle simultaneously, a phase diagram on these two factors is plotted in Fig. 10 according to whether the hydraulic fracture is able to cross the cemented natural fracture. It can be seen that for both weakly (see Fig. 10a) and strongly (see Fig. 10b) cemented natural fractures, a smaller strength contrast or a larger approach angle is more conducive to the penetration process, which includes two implications.

Firstly, hydraulic fracture more easily crosses the cemented natural fracture at high approach angle. For example, in rocks with strength ratio being 0.5 (No. 2, 8, and 14 in Fig. 9), with the increment of approach angle, the interaction process transforms from deflection (No. 14 in Fig. 9) to penetration (No. 2 and 8 in Fig. 9). Similar results were also observed in other numerical and experimental study (Lee et al., 2015; Virgo et al., 2013).

Secondly, deflection process more easily happens in rocks with large

strength contrast. For example, when approach angle is equal to  $60^\circ$  (No. 7, 8, 9, 10, 11, and 12 in Fig. 9), with the increment of strength ratio, strength contrast first decreases and then increases. As a result, the interaction process shifts from deflection (No. 7 in Fig. 9) to penetration (No. 8, 9, 10 and 11 in Fig. 9) and finally returns to deflection again (No. 12 in Fig. 9).

It should be noted that although deflection process also happens in rocks with strongly cemented natural fracture, the involved mechanisms are different from that in rocks with weakly cemented natural fracture. In weakly cemented fracture cases, deflection is caused by the shear slippage in weakly cemented fracture (see Fig. 7b). However, in rocks with strongly cemented natural fracture, hydraulic fracture diverts and propagates in host rock along the cement wall (see Fig. 11b), where tensile failure more easily happens. This fracturing behavior is attributed to the high tensile strength of cement material in strongly cemented natural fracture. The same feature was also observed in natural structure as presented in Fig. 11c (Virgo et al., 2013), where the right fracture is a pre-existing one filled with minerals, and when a new fracture encounters it, deflection process happens.

### 3.1.4. Comparison with bonded interface

In previous study, natural fracture is often treated as a frictional or bonded interface. As a comparison, cemented natural fracture in this part is also represented by a bonded interface with no cement material (red dash line in Fig. 12), and the host rock properties on both sides of the interface are same (blue part in Fig. 12). The strength ratio is defined as the ratio of bonded interface strength to host rock strength, and other parameters are same as those in Section 3.1.3.

Similar to the classification in Section 3.1.3, hydraulic fractures in rock with bonded interface (see Fig. 12) are also grouped into deflection and penetration process as shown in Fig. 13. In rocks with weakly bonded interface, large approach angle or small strength contrast facilitates the penetration process (see Fig. 13a), which is consistent with the conclusion obtained in Section 3.1.3 where cement material is considered explicitly (see Fig. 10a). However, in rocks with strongly bonded interface, all the hydraulic fractures can across the interface (see Fig. 13b), which conflicts with the observation in natural structure (Fig. 11c). It is because bonded interface can only accommodate shear force in tangential direction and tensile force in normal direction to itself. However, high tensile strength of cement material in both tangential and normal directions is a typical feature of strongly cemented natural fracture, which results in the deflection process (see Fig. 11), but this feature cannot be captured in bonded interface model. Current results provide a direct evidence that previous conclusions obtained from hydraulic fracture interaction with frictional or bonded interface cannot be directly applied to the cemented natural fracture cases. Thus, it is necessary and critical to explore the hydraulic fracture propagation in rock with cemented natural fracture.

## 3.2. Multi cemented fractures

The above discussions are based on single cemented natural fracture, and in this part hydraulic fracture propagation in rock with multi cemented natural fractures is simulated, which is closer to the real application. In current simulation, rock with randomly distributed multi cemented natural fractures is generated by quartet structure generation set (QSGS), which is an efficient method to generate random but statistically representative multiphase materials (i.e. porous media and composite material etc.) (Wang and Pan, 2008; Wang et al., 2007).

Here, two groups of samples are considered: multi cemented natural fractures are parallel or orthogonal to the hydraulic fracture propagation direction. In each group, five samples with same volume fraction of cemented natural fractures are generated to get the general conclusion (see Fig. 14). Two strength ratios (0.33 and 4.0) are used to represent weakly and strongly cemented natural fractures respectively.

### 3.2.1. Weakly cemented fracture effect

Hydraulic fractures in rocks with multi weakly cemented natural fractures (strength ratio = 0.33) are presented in Fig. 15, which shows that hydraulic fracture geometries in orthogonal cases are much more complex than those in parallel cases. In order to get a quantitative comparison of fracture complexity between these two cases, connected fracture networks in Fig. 15 are extracted (see Fig. 16a–b), and their modified topological indexes ( $q_m$ ) are calculated (see Fig. 16c). Modified topological index ( $q_m$ ) is a parameter to quantify the complexity of fracture geometry (Chen and Wang, 2017), whose range is between 0 and 1, and smaller  $q_m$  corresponds to a more complex fracture geometry. Modified topological indexes ( $q_m$ ) in orthogonal cases are smaller than those in parallel cases (see Fig. 16c), which quantitatively demonstrates that complex fracture network is more easily formed in rocks where multi weakly cemented natural fractures are orthogonal to the hydraulic fracture propagation direction.

In orthogonal cases, hydraulic fracture arrested by the weakly cemented natural fracture can penetrate into the host rock again at the end of weakly cemented fracture (see Fig. 15a). Then it may encounter other weakly cemented natural fractures and repeat the above processes. It is repeated deflection and penetration processes that result in the complex fracture geometry in orthogonal cases. Similar result was also reported in Warpinski and Teufel (1987). However, in parallel cases, weakly cemented natural fractures are difficult to be connected with each other. As a result, only a simple fracture can be induced (see Fig. 16b).

### 3.2.2. Strongly cemented fracture effect

Fig. 17 shows the hydraulic fracture propagation in rocks with multi strongly cemented natural fractures, where complex fracture network cannot be formed. In orthogonal cases, hydraulic fracture may bypass or penetrate the strongly cemented fracture, and deflection process is not observed, because high energy is required for hydraulic fracture to deflect  $90^\circ$ . An interesting interaction process, crack jump, is observed in last two subfigures of Fig. 17a. When hydraulic fracture encounters the strongly cemented natural fracture orthogonally, it is able to “cross” the strongly cemented fracture by re-initiating a secondary fracture on the other side of strongly cemented fracture without actually breaking it. There are two reasons, firstly stress concentration around the tip of primary fracture can re-initiate a new discontinuous fracture (Virgo et al., 2013). Secondly, fluid can move through the strongly cemented fracture without breaking it, which results in the high fluid pressure in the surrounding host rock and hence inducing a secondary fracture (Olson et al., 2012). For parallel cases, the interaction process is simple, and all the hydraulic fractures bypass the strongly cemented natural fractures (Fig. 17b). It is because hydraulic fracture prefers to propagate around the strongly cemented natural fractures owing to the relatively low resistance in the surrounding host rock, and the small height of cemented fractures in parallel cases facilitates this behavior.

## 4. Conclusion

In this study, a pore-scale LBM-DEM model developed by our previous work for hydro-mechanical coupled mechanism is applied to investigate the hydraulic fracture propagation in rocks with cemented natural fractures. Particular emphasis is put on the effects from both fracture-matrix strength ratio and hydraulic-natural approach angle. Beyond the traditional continuum-based models, this discrete model enables us to predict the complex hydraulic fracture geometry directly and reveal the micro failure mechanism explicitly. The results show that two possible interaction processes, deflection and penetration, are observed, which are determined by the strength ratio (between cemented natural fracture and host rock) and approach angle (between hydraulic and cemented natural fracture). A larger strength contrast or a smaller approach angle is more conducive to the deflection in rocks with weakly or strongly cemented natural fracture, which is consistent with experimental observations. In addition, in rocks with multiple cemented natural fractures, complex

fracture network is more easily induced when hydraulic fracture propagation direction is orthogonal to the weakly cemented fractures.

Current numerical results provide some basic understanding of hydraulic fracture propagation in rocks with cemented natural fractures, including the involved failure mechanism and the induced fracture geometry.

- (i) In rocks with weakly cemented natural fractures, penetration or deflection process is determined by the competition of shear failure in weakly cemented fracture and tensile failure in surrounding host rock. If shear slippage in weakly cemented fracture occurs before tensile stress in host rock reaches its tensile strength, deflection process happens and shear failure dominates this process. Otherwise, penetration process happens. In rocks with strongly cemented natural fractures, large strength contrast and small approach angle can also result in deflection just like the observation in natural structure from Oman Mountain, but the mechanism is not same as that in rocks with weakly cemented fractures. In this case, when strongly cemented natural fracture is encountered, hydraulic fracture deflects and propagates in host rock along the cement wall, where tensile failure more easily happens. This deflection process in rocks with strongly cemented natural fractures cannot be captured by the previous models, where the cemented natural fracture was treated as a bonded interface, because bonded interface cannot accommodate tensile stress in tangential direction to itself. Thus, for rocks with strongly cemented natural fractures, cement material in the natural fracture should be represented explicitly rather than replaced by an equivalent bonded force with zero thickness.
- (ii) Multiple weakly cemented natural fractures orthogonal to the hydraulic fracture propagation direction can facilitate the formation of complex fracture geometry by repeated deflection and penetration process. However, if weakly cemented natural fractures are parallel to the hydraulic fracture propagation direction, complex fracture network cannot be induced, because weakly cemented natural fractures are difficult to be connected with each other. Thus, in order to improve the efficiency of hydraulic fracture treatment, the induced main hydraulic fracture is suggested to be orthogonal to the weakly cemented natural fractures in formation, because for unconventional reservoirs complex fracture network may help to achieve commercial production.

## Acknowledgements

This work is financially supported by the NSFC-DFG Collaboration Grant (No. 11761131012) grant, the NSF grant of China (No. U1562217) and National Science and Technology Major Project on Oil and Gas (No.2017ZX05013001). The authors want to acknowledge the open source library MechSys developed by S. A. Galindo Torres (<http://mechsys.nongnu.org/index.shtml>).

## References

- Al-Busaidi, A., Hazzard, J., Young, R., 2005. Distinct element modeling of hydraulically fractured Lac du Bonnet granite. *J. Geophys. Res. Solid Earth* 110, B06302.
- Alabbad, E.A., Olson, J.E., 2016. Examining the geomechanical implications of pre-existing fractures and simultaneous-multi-fracturing completions on hydraulic fractures: experimental insights into fracturing unconventional formations. In: SPE Annual Technical Conference and Exhibition.
- Bahorich, B., Olson, J.E., Holder, J., 2012. Examining the effect of cemented natural fractures on hydraulic fracture propagation in hydrostone block experiments. In: SPE Annual Technical Conference and Exhibition.
- Behraftar, S., Torres, S.G., Scheuermann, A., Williams, D., Marques, E., Avarzaman, H.J., 2017. A calibration methodology to obtain material parameters for the representation of fracture mechanics based on discrete element simulations. *Comput. Geotech.* 81, 274–283.
- Blanton, T.L., 1982. An experimental study of interaction between hydraulically induced and pre-existing fractures. In: SPE Unconventional Gas Recovery Symposium.
- Boutt, D., Cook, B., Williams, J., 2011. A coupled fluid–solid model for problems in geomechanics: application to sand production. *Int. J. Numer. Anal. Meth.* 35 (9), 997–1018.
- Chen, S., Doolen, G.D., 1998. Lattice Boltzmann method for fluid flows. *Annu. Rev. Fluid Mech.* 30 (1), 329–364.
- Chen, Z., Wang, M., 2017. Pore-scale modeling of hydromechanical coupled mechanics in hydrofracturing process. *J. Geophys. Res. Solid Earth* 122 (5), 3410–3429.
- Chen, Z., Xie, C., Chen, Y., Wang, M., 2016. Bonding strength effects in hydro-mechanical coupling transport in granular porous media by pore-scale modeling. *Computation* 4 (1), 15.
- Cundall, P.A., Strack, O.D., 1979. A discrete numerical model for granular assemblies. *Geotechnique* 29 (1), 47–65.
- Cunfei, M., Chummei, D., Guoqiang, L., Chengyan, L., Xiaocen, L., Elsworth, D., 2016. Types, characteristics and effects of natural fluid pressure fractures in shale: a case study of the Paleogene strata in Eastern China. *Petrol. Explor. Dev.* 43 (4), 634–643.
- Economides, M.J., Nolte, K.G., 2000. *Reservoir Stimulation*. Wiley New York.
- Fisher, M.K., Wright, C.A., Davidson, B.M., Goodwin, A., Fielder, E., Buckler, W., Steinsberger, N., 2002. Integrating fracture mapping technologies to optimize stimulations in the Barnett Shale. In: SPE Annual Technical Conference and Exhibition.
- Gale, J.F., Holder, J., 2010. Natural fractures in some US shales and their importance for gas production. In: Geological Society, London, Petroleum Geology Conference Series. Geological Society of London, pp. 1131–1140.
- Gale, J.F., Laubach, S.E., Marrett, R.A., Olson, J.E., Holder, J., Reed, R.M., 2004. Predicting and characterizing fractures in dolostone reservoirs: using the link between diagenesis and fracturing. *Geol. Soc. Lond. Spec. Publ.* 235 (1), 177–192.
- Gale, J.F., Laubach, S.E., Olson, J.E., Eichhubl, P., Fall, A., 2014. Natural fractures in shale: a review and new observations. *AAPG Bull.* 98 (11), 2165–2216.
- Gale, J.F., Reed, R.M., Holder, J., 2007. Natural fractures in the Barnett Shale and their importance for hydraulic fracture treatments. *AAPG Bull.* 91 (4), 603–622.
- Galindo-Torres, S., 2013. A coupled Discrete Element Lattice Boltzmann Method for the simulation of fluid–solid interaction with particles of general shapes. *Comput. Meth. Appl. Mech. Eng.* 265, 107–119.
- Galindo-Torres, S., Pedroso, D., Williams, D., Li, L., 2012. Breaking processes in three-dimensional bonded granular materials with general shapes. *Comput. Phys. Commun.* 183 (2), 266–277.
- Gasparrini, M., Sassi, W., Gale, J.F., 2014. Natural sealed fractures in mudrocks: a case study tied to burial history from the Barnett Shale, Fort Worth Basin, Texas, USA. *Mar. Petrol. Geol.* 55, 122–141.
- Gu, H., Weng, X., Lund, J.B., Mack, M.G., Ganguly, U., Suarez-Rivera, R., 2012. Hydraulic fracture crossing natural fracture at nonorthogonal angles: a criterion and its validation. *SPE Prod. Oper.* 27 (01), 20–26.
- He, X., Guo, Y., Li, M., Pan, N., Wang, M., 2017. Effective gas diffusion coefficient in fibrous materials by mesoscopic modeling. *Int. J. Heat Mass Tran.* 107, 736–746.
- Laubach, S., Diaz-Tushman, K., 2009. Laurentian palaeostress trajectories and ephemeral fracture permeability, Cambrian Eriboll Formation sandstones west of the Moine Thrust Zone, NW Scotland. *J. Geol. Soc.* 166 (2), 349–362.
- Lee, H., Olson, J., Schultz, R., 2016. The interaction analysis of propagating opening mode fractures with veins using discrete element method. In: 50th US Rock Mechanics/Geomechanics Symposium.
- Lee, H.P., Olson, J.E., Holder, J., Gale, J.F., Myers, R.D., 2015. The interaction of propagating opening mode fractures with preexisting discontinuities in shale. *J. Geophys. Res. Solid Earth* 120 (1), 169–181.
- Maxwell, S.C., Urbancic, T., Steinsberger, N., Zinno, R., 2002. Microseismic imaging of hydraulic fracture complexity in the Barnett shale. In: SPE Annual Technical Conference and Exhibition.
- Mayerhofer, M.J., Lolon, E., Warpinski, N.R., Cipolla, C.L., Walsler, D.W., Rightmire, C.M., 2010. What is stimulated reservoir volume? *SPE Prod. Oper.* 25 (01), 89–98.
- Noble, D., Torczynski, J., 1998. A lattice-Boltzmann method for partially saturated computational cells. *Int. J. Mod. Phys. C* 9 (08), 1189–1201.
- Olson, J.E., Bahorich, B., Holder, J., 2012. Examining hydraulic fracture: natural fracture interaction in hydrostone block experiments. In: SPE Hydraulic Fracturing Technology Conference.
- Renshaw, C., Pollard, D., 1995. An experimentally verified criterion for propagation across unbounded frictional interfaces in brittle, linear elastic materials. *Int. J. Rock Mech. Min. Sci. Geomech. Abstr.* 32 (3), 237–249.
- Strack, O.E., Cook, B.K., 2007. Three-dimensional immersed boundary conditions for moving solids in the lattice-Boltzmann method. *Int. J. Numer. Meth. Fluid.* 55 (2), 103–125.
- Virgo, S., Abe, S., Urai, J.L., 2013. Extension fracture propagation in rocks with veins: insight into the crack-seal process using Discrete Element Method modeling. *J. Geophys. Res. Solid Earth* 118 (10), 5236–5251.
- Virgo, S., Abe, S., Urai, J.L., 2014. The evolution of crack seal vein and fracture networks in an evolving stress field: insights from Discrete Element Models of fracture sealing. *J. Geophys. Res. Solid Earth* 119 (12), 8708–8727.
- Wang, L., Yao, B., Xie, H., Winterfeld, P.H., Kneafsey, T.J., Yin, X., Wu, Y.-S., 2017. CO<sub>2</sub> injection-induced fracturing in naturally fractured shale rocks. *Energy* 139, 1094–1110.
- Wang, M., Pan, N., 2008. Predictions of effective physical properties of complex multiphase materials. *Mater. Sci. Eng. R Rep.* 63 (1), 1–30.
- Wang, M., Wang, J., Pan, N., Chen, S., 2007. Mesoscopic predictions of the effective thermal conductivity for microscale random porous media. *Phys. Rev. E* 75 (3), 036702.
- Wang, Z., Jin, X., Wang, X., Sun, L., Wang, M., 2016. Pore-scale geometry effects on gas permeability in shale. *J. Nat. Gas Sci. Eng.* 34, 948–957.

- Warpinski, N., Teufel, L., 1987. Influence of geologic discontinuities on hydraulic fracture propagation. *J. Pet. Technol.* 39 (02), 209–220.
- Weng, X., Kresse, O., Cohen, C.-E., Wu, R., Gu, H., 2011. Modeling of hydraulic-fracture-network propagation in a naturally fractured formation. *SPE Prod. Oper.* 26 (04), 368–380.
- Xie, C., Zhang, J., Bertola, V., Wang, M., 2016. Lattice Boltzmann modeling for multiphase viscoplastic fluid flow. *J. Non-Newtonian Fluid Mech.* 234, 118–128.
- Zhang, X., Sanderson, D.J., Barker, A.J., 2002. Numerical study of fluid flow of deforming fractured rocks using dual permeability model. *Geophys. J. Int.* 151 (2), 452–468.